

Interplay between Superconductivity and Altermagnetism in Disordered Materials and Heterostructures

Rodrigo de las Heras^{1,*}, Tim Kokkeler^{2,†}, Stefan Ilić², Ilya V. Tokatly^{3,4,5} and F. Sebastian Bergeret^{1,3}

¹*Centro de Física de Materiales (CFM-MPC) Centro Mixto CSIC-UPV/EHU, E-20018 Donostia-San Sebastián, Spain*

²*Department of Physics and Nanoscience Center, University of Jyväskylä,*

P.O. Box 35 (YFL), FI-40014 University of Jyväskylä, Finland

³*Donostia International Physics Center (DIPC), 20018 Donostia-San Sebastián, Spain*

⁴*Departamento de Polímeros y Materiales Avanzados,*

Universidad del País Vasco UPV/EHU, 20018 Donostia-San Sebastián, Spain

⁵*IKERBASQUE, Basque Foundation for Science, 48009 Bilbao, Spain*

We study the interplay between superconductivity and altermagnetism in disordered systems using recently derived quantum kinetic transport equations. Starting from this framework, we derive the Ginzburg–Landau free energy and identify, in addition to the conventional pair-breaking term, a coupling between the spin and the spatial variation of the superconducting order parameter. Two distinct effects emerge from this coupling. The first is a magnetoelectric effect, in which a supercurrent (*i.e.*, a phase gradient) induces a spin texture; this contribution is quadratic in the phase gradient. The second effect arises when the magnitude, rather than the phase, of the superconducting order parameter varies in space, likewise leading to a finite magnetization. We show that these two contributions compete in the case of an Abrikosov vortex, where both the amplitude and phase of the order parameter vary spatially. The effect associated with amplitude variations also gives rise to a proximity-induced magnetization (PIM) in hybrid structures composed of a superconductor (S) and an altermagnet (AM). Using quasiclassical theory, we analyze the PIM in diffusive S/AM bilayers and S/AM/S Josephson junctions, and determine the induced magnetization profiles. In Josephson junctions, where both the PIM and the magnetoelectric effect coexist, we further predict the occurrence of $0-\pi$ transitions.

I. INTRODUCTION

A recent development in condensed matter physics that attracts considerable attention is the prediction of altermagnets [1, 2], a class of materials combining antiferromagnetic type of spin distribution (zero net magnetization per unit cell) with spin-split electronic bands. This unique combination makes them promising candidates for spintronics applications, where they can exhibit intriguing transport phenomena [3–7].

An equally interesting research direction is the combination of altermagnetism and superconductivity [8–20], both in coexisting situations and in hybrid structures. Most of these works focus on purely ballistic systems. However, a recent work [21] derives the kinetic equations describing transport in normal and superconducting diffusive systems with altermagnets. These equations were obtained from the nonlinear sigma model (NLSM) developed in Ref. [21] using a symmetry-based approach [22].

In this work, we use the framework of Ref. [21] to explore the interplay between superconductivity and altermagnetism in diffusive systems. First, we derive from the NLSM the Ginzburg–Landau (GL) free-energy functional for a disordered superconducting altermagnet. The simple structure of this functional reveals that, besides the exchange-field-induced pair-breaking

mechanisms that renormalize the usual GL coefficients, a new term emerges, associated with the altermagnetic order. This term is of the second order in the gradients of the order parameter and is closely related to the phenomenon of piezomagnetism [23].

It is known that d -wave altermagnets allow for a linear piezomagnetic effect [24, 25], that is, a linear relation $M_i = \alpha_{ijk} u_{jk}$ between the magnetization M_i and the strain tensor u_{jk} . In other words, the symmetry of altermagnets implies the existence of a third rank tensor α_{ijk} which is odd under time reversal and symmetric in its last two indices. An immediate consequence is that, in the superconducting state, such materials may exhibit a magnetization induced by inhomogeneities of the order parameter, $M_i \sim \alpha_{ijk} (\partial_j \Delta) (\partial_k \Delta^*)$. As we show below, the GL functional derived from the NLSM indeed contains precisely such a term, arising naturally from the symmetry-based approach of Ref. [21].

This gradient term contains two distinct physical mechanisms. First, the magnetoelectric effect predicted in [9, 10], in which a phase gradient, *i.e.*, a supercurrent, induces a magnetic moment. Symmetry dictates that this effect appears only at second order in the phase gradient. Second, our analysis shows that the same term also describes a distinct effect in which a finite magnetization arises when the *magnitude*, rather than the *phase*, of the order parameter varies in space. Such an effect should manifest in materials where superconductivity and altermagnetism coexist and the order parameter is real and spatially inhomogeneous, as in a Larkin–Ovchinnikov-type phase.

* rodrigo.delasheras@ehu.eus

† tim.h.kokkeler@jyu.fi

Moreover, the latter effect is also expected in a hybrid S/AM bilayers, where superconducting correlations penetrate into the altermagnet via the proximity effect, decaying away from the S/AM interface and thereby generating a finite magnetic moment even in the absence of an injected supercurrent. In this geometry, the presence of a normal vector to the S/AM interface allows this effect to appear already to first order in the magnitude gradient. We refer to this mechanism as a proximity-induced magnetization (PIM). The generated magnetization is an emergent property of the hybrid junction, since both the superconductor and the altermagnet intrinsically lack a net magnetic moment.

With the help of the Usadel equation for altermagnets, we present an exhaustive analysis of the proximity-induced magnetization (PIM), first in an S/AM bilayer. We derive the characteristic length of the superconducting proximity effect in altermagnets, which depends on both the altermagnetic parameter K and the pair-breaking rate Γ . As in ferromagnets [26], the superconducting condensate not only decays inside the AM but also oscillates in space. Within the same framework, we also analyze the PIM in an S/AM/S Josephson junction and determine the critical current as a function of the material parameters. When a supercurrent is induced in the junction, the PIM coexists with the magnetoelectric effect, which is quadratic in the phase difference between the superconducting leads. We also find that $0-\pi$ transitions are possible in such systems, for example, upon varying the temperature.

Our analysis is based on general equations valid for any microscopic realization of an altermagnet. As an example we also include a specific effective low-energy Hamiltonian describing a disordered system with coexisting superconducting and altermagnetic order. From this Hamiltonian, we derive in Appendix A the quasiclassical equations in the diffusive limit and establish the connection between the effective parameters of the nonlinear sigma model.

The paper is organized as follows. In Section II, we present the Ginzburg–Landau free energy for a superconducting altermagnet and highlight the main effects arising from the interplay between superconducting and altermagnetic orders. In Section III, we analyze the proximity-induced magnetization (PIM) in S/AM and S/AM/S structures. For S/AM/S Josephson junctions, we show that the magnetization arises both from the supercurrent and from spatial variations of the modulus of the superconducting condensate, and we discuss the possibility of $0-\pi$ transitions in the Josephson current. In Section IV, we express the parameters of the altermagnet in terms of an effective low-energy model describing altermagnetic order. Finally, we summarize our conclusions in Section V.

II. GINZBURG–LANDAU FREE ENERGY

In this section we derive the Ginzburg–Landau (GL) free energy for a dirty superconducting altermagnet. Our starting point is the expression for the free energy functional [27]:

$$F = \frac{\nu_0}{\lambda} |\Delta|^2 - T \sum_{n=-\infty}^{\infty} iS[\tilde{g}, \omega_n], \quad (1)$$

where here λ is the phonon-mediated pairing interaction constant, ν_0 the density of states per spin at the Fermi level, T the temperature and Δ the superconducting order parameter. The second term in Eq. (1), including terms due to superconductivity and altermagnetism, reads [21]:

$$\begin{aligned} iS[\tilde{g}, \omega_n] = & \frac{\pi\nu_0}{2} \text{Tr} \left(-\frac{D}{4} (\tilde{\nabla}\tilde{g})^2 + \omega_n \tilde{\tau}_3 \tilde{g} + \tilde{\Delta} \tilde{g} \right. \\ & + \frac{1}{4} \Gamma_{ab} \tilde{\tau}_3 \hat{\sigma}_a \tilde{g} \tilde{\tau}_3 \hat{\sigma}_b \tilde{g} + \frac{D}{4} T_{ajk} \hat{\sigma}_a \tilde{\tau}_3 \tilde{\nabla}_j \tilde{g} \tilde{\nabla}_k \tilde{g} \\ & \left. - \frac{iD}{4} K_{ajk} \hat{\sigma}_a \tilde{\tau}_3 \tilde{g} \tilde{\nabla}_j \tilde{g} \tilde{\nabla}_k \tilde{g} + ig\mu_B B_a \hat{\sigma}_a \tilde{\tau}_3 \tilde{g} \right). \end{aligned} \quad (2)$$

The above expression corresponds to the Luttinger–Ward functional in terms of the quasiclassical Green’s function \tilde{g} [27]. In fact, it is the saddle point value of the effective action of the NLSM for an equilibrium superconductor¹. It has a 4×4 matrix structure in Nambu–spin space [28], and satisfies the normalization condition $\tilde{g}^2 = 1$. The specific structure of the tensors in Eq. (2) is determined purely by symmetry, in the same spirit as the construction of the nonlinear sigma model (NLSM) recently proposed in Refs. [21, 22].

In Eq. (2), D is the diffusion coefficient, $\omega_n = \pi T(1 + 2n)$ the Matsubara frequencies, $\tilde{\Delta} = |\Delta| \tilde{\tau}_1 e^{i\tilde{\tau}_3 \varphi}$ the matrix pair potential and φ the phase of the superconductor. We introduce the covariant derivative $\tilde{\nabla}_k \tilde{Q} = \partial_k \tilde{Q} - iA_k [\tilde{\tau}_3, \tilde{Q}]$ where A_k is the vector potential, μ_B the Bohr magneton, g the Landé g -factor and $B_i = \varepsilon_{ijk} \partial_j A_k$ an external magnetic field.

The tensors Γ_{ab} , K_{ajk} , and T_{ajk} describe different aspects of exchange interactions in magnetic materials. The tensor Γ_{ab} represents a spin-relaxation term associated with magnetic interactions, and is present in ferromagnets, antiferromagnets and altermagnets. The tensors K_{ajk} and T_{ajk} , are odd under time-reversal symmetry and symmetric in the last two indices. They describe the physics of spin-dependent transport phenomena [21]. Specifically, T_{ajk} is related to the difference in diffusion constant for electrons with

¹ Technically, in the NLSM one should restrict the time integration to the forward branch of the contour to obtain the connection to the free energy.

opposite spin along the collinear axis, while K_{ajk} to the Larmor precession in the presence of gradients [21]. Consequently, T_{ajk} and K_{ajk} , only appear in systems with spin-split bands, such as ferromagnets and altermagnets, but vanish in antiferromagnets, where the absence of spin splitting forbids them by symmetry.

A key distinction between ferromagnets and altermagnets lies in the presence of a net exchange field. In ferromagnets, this would give rise to an additional term $ih_a^F \hat{\sigma}_a \tilde{\tau}_3 \tilde{g}$ in Eq. (2), associated with the finite exchange field h_a^F . In altermagnets, however, the total exchange field averages to zero, so such a term cannot appear intrinsically; it can only be generated by applying an external magnetic field B_a . Therefore, while spin phenomena in ferromagnets are primarily governed by h_a^F , in altermagnets the dominant spin-related effects originate from the tensors K_{ajk} and T_{ajk} .

Minimization of the energy Eq. (1) with respect to \check{g} gives the Usadel equation:

$$\check{\nabla}_k \check{J}_k = [\check{g}, (\omega_n + ig\mu_B B_a \hat{\sigma}_a) \tilde{\tau}_3 + \check{\Delta}] + \frac{1}{2} \Gamma_{ab} [\check{g}, \tilde{\tau}_3 \hat{\sigma}_a \check{g} \tilde{\tau}_3 \hat{\sigma}_b] + \check{T}, \quad (3)$$

where summation over repeated indices is implied. The matrix current \check{J}_k and torque \check{T} are position and Matsubara frequency dependent matrices in Nambu-spin space, given by:

$$\check{J}_k = -D \left(\check{g} \check{\nabla}_k \check{g} - \frac{1}{4} T_{ajk} \{ \tilde{\tau}_3 \hat{\sigma}_a + \check{g} \tilde{\tau}_3 \hat{\sigma}_a \check{g}, \check{g} \check{\nabla}_j \check{g} \} + \frac{i}{4} K_{ajk} [\tilde{\tau}_3 \hat{\sigma}_a + \check{g} \tilde{\tau}_3 \hat{\sigma}_a \check{g}, \check{\nabla}_j \check{g}] \right) \quad (4)$$

$$\check{T} = D \left(\frac{1}{4} T_{jk} [\tilde{\tau}_3 \hat{\sigma}_a, \check{\nabla}_j \check{g} \check{\nabla}_k \check{g}] + \frac{i}{4} K_{jk} [\tilde{\tau}_3 \hat{\sigma}_a, \check{g} \check{\nabla}_j \check{g} \check{\nabla}_k \check{g}] \right). \quad (5)$$

It is important to emphasize that the Usadel equation, Eq. (3), is formulated solely on the basis of symmetry considerations. As a result, all symmetry-allowed terms appear as independent phenomenological coefficients. In Section IV, we derive these coefficients from a specific low-energy Hamiltonian, thereby confirming its general structure and providing expressions for the coefficients in terms of the parameters of that particular realization.

To derive the Ginzburg–Landau (GL) free energy we consider a bulk superconductor with altermagnetic order near its critical temperature T_c . Close to T_c the Usadel equation Eq. (3) can be linearized, and the Green's function parametrized as:

$$\check{g} = \begin{pmatrix} \text{sgn}(\omega_n)(1 - \frac{1}{2} \hat{f} \hat{f}) & \hat{f} \\ \hat{f} & -\text{sgn}(\omega_n)(1 - \frac{1}{2} \hat{f} \hat{f}) \end{pmatrix}, \quad (6)$$

where \hat{f} and $\hat{\hat{f}}$ are the anomalous Green's functions in spin space that describe the condensate. They decompose as:

$$\hat{f} = f_s + f_t^a \hat{\sigma}_a, \quad \hat{\hat{f}} = \tilde{f}_s + \tilde{f}_t^a \hat{\sigma}_a. \quad (7)$$

where f_s is the singlet component of the condensate and f_t^a the triplet components.

Substituting this parametrization into the Usadel equation, assuming that only $\Gamma_{zz} \equiv \Gamma \neq 0$ (which is motivated in section IV), neglecting spatial derivatives (bulk limit) and to linear order in Δ and B_a , one finds:

$$f_s = \frac{\Delta}{|\omega_n| + \Gamma}, \quad \tilde{f}_s = \frac{\Delta^*}{|\omega_n| + \Gamma}, \quad (8)$$

$$f_t^a = -\frac{i \text{sgn}(\omega_n) \Delta}{(|\omega_n| + \Gamma)^2} g \mu_B B_a, \quad \tilde{f}_t^a = -\frac{i \text{sgn}(\omega_n) \Delta^*}{(|\omega_n| + \Gamma)^2} g \mu_B B_a. \quad (9)$$

Inserting these solutions into Eq. (1), and keeping terms up to second order in $|\Delta|$ and linear order in B_a , gives the GL functional:

$$F = F_n + a|\Delta|^2 + c|\Pi\Delta|^2 + c' B_a K_{ajk} \Pi_j \Delta \Pi_k^* \Delta^* + O(|\Delta|^4) + O(B_a^2), \quad (10)$$

where $\Pi_j = -i\partial_j - 2A_j$, F_n is the free energy of the normal state and:

$$a = \frac{\nu_0}{\lambda} - 2\pi\nu_0 T \sum_{n=0}^{n_{max}} \frac{1}{\omega_n + \Gamma}, \quad (11)$$

$$c = \pi\nu_0 T \sum_{n=0}^{\infty} \frac{D}{(\omega_n + \Gamma)^2}, \quad (12)$$

$$c' = \pi\nu_0 T \sum_{n=0}^{\infty} \frac{2D}{(\omega_n + \Gamma)^3}, \quad (13)$$

where in Eq. (11), we introduce the Debye frequency as a cutoff $n_{max} = \omega_D/(2\pi T)$.

The resulting free energy coincides in structure with the Ginzburg–Landau functional presented in Ref. [10]. However, our derivation establishes a connection between the corresponding GL coefficients and the parameters of the higher level Usadel theory that is valid for any temperature.

Note that the tensor T_{ajk} in Eqs. (3-5) does not enter the free energy, *i.e.*, it does not contribute to equilibrium properties in single domain superconducting collinear altermagnets, in agreement with Ref. [21].

At $T = T_c$, the coefficient a must vanish, and therefore:

$$\frac{1}{\lambda} = 2\pi T_c \sum_{n=0}^{n_{max}} \frac{1}{\omega_n + \Gamma}. \quad (14)$$

By subtracting the equivalent equation for zero Γ , one obtains the expression determining the critical temperature:

$$\begin{aligned} \ln\left(\frac{T_c}{T_{c0}}\right) &= 2\pi T_c \sum_{n=0}^{\infty} \left(\frac{1}{\omega_n + \Gamma} - \frac{1}{\omega_n} \right) \\ &= \psi^{(0)}\left(\frac{1}{2}\right) - \psi^{(0)}\left(\frac{1}{2} + \frac{\Gamma}{2\pi T_c}\right), \end{aligned} \quad (15)$$

where T_{c0} is the critical temperature in the absence of Γ . Equation (15) is formally identical to the Abrikosov–Gor’kov theory of magnetic impurities in superconductors [29], with Γ being the pair-breaking parameter.

More interesting is the last term in the first line of Eq. (10), proportional to the tensor K_{ajk} . This term couples order-parameter gradients to spin polarization, leading to a finite magnetization, which can be obtained by differentiating the free energy with respect to B_a [30]:

$$M_a = -\frac{\partial F}{\partial B_a} = -\sum_{n=0}^{\infty} \frac{2g\mu_B\nu_0\pi TD}{(\omega_n + \Gamma)^3} K_{ajk} \Pi_j \Delta \Pi_k^* \Delta^* \\ = \frac{g\mu_B\nu_0 D}{8\pi^2 T^2} \psi^{(2)} \left(\frac{1}{2} + \frac{\Gamma}{2\pi T} \right) K_{ajk} \Pi_j \Delta \Pi_k^* \Delta^*. \quad (16)$$

where $\psi^{(2)}(z)$ is the tetragamma function [31]. The induced magnetization is proportional to the tensor K_{ajk} and decreases with increasing Γ , since $\psi^{(2)}(z)$ is a monotonically decreasing function for $z > 0$. It is worth noting that the existence of the term proportional to the K -tensor in the GL functional, Eq. (10), for a superconductor with altermagnetic order can also be justified solely on the basis of symmetry arguments.

Eq. (16) predicts the appearance of a finite magnetization arising from the spatial variation of the order parameter $\Delta(\mathbf{r})$. One can distinguish two situations. The first arises when $|\Delta|$ is constant in space but we have a finite phase gradient $\partial_k \varphi$. This describes the magnetoelectric effect, previously discussed in Refs. [9, 10], corresponding to a magnetic moment induced by a supercurrent. Importantly, unlike the conventional Edelstein effect in superconductors with spin–orbit coupling [32], this response is nonlinear in the phase gradient; the induced magnetization scales quadratically with the supercurrent. For this reason, it is referred to as the nonlinear superconducting magnetoelectric effect [9, 33]².

The second situation, described by Eq. (16), corresponds to the appearance of a magnetization in the presence of spatial variations of the magnitude $\partial_k |\Delta|$, but not of its phase. In other words, even in the absence of any supercurrent, a magnetization may be induced. Such variations occur, for example, in inhomogeneous superconductors with a real order parameter, as in Larkin–Ovchinnikov phase [35].

An interesting example that illustrates both types of effects, *i.e.*, the induced magnetization due to the

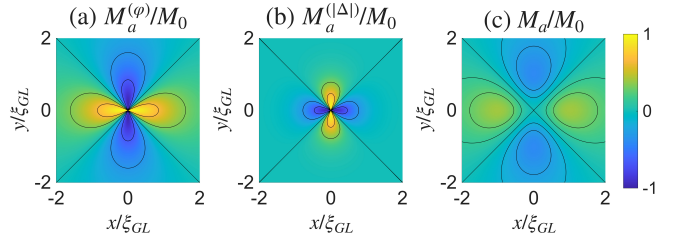


Figure 1. Magnetization induced in the presence of an Abrikosov vortex in a superconducting altermagnet with vorticity $m = 1$. Contributions due to (a) the nonlinear magnetoelectric effect, and (b) due to the variation of $|\Delta|$. (c) Total magnetization $M_a = M_a^{(\varphi)} + M_a^{(|\Delta|)}$. The underlying d -wave symmetry of the altermagnet is manifested as four lobes with alternating sign.

nonlinear magnetoelectric effect and that arising from an inhomogeneous order parameter, is the case of an Abrikosov vortex. In such a case, the order parameter can be approximated by $\Delta(\mathbf{r}) \approx \tanh(r/\xi_{GL}) e^{im\varphi}$, where $r = \sqrt{x^2 + y^2}$, $\varphi = \arctan(y/x)$, ξ_{GL} is the coherence length, and $m = \pm 1, \pm 2, \dots$ is the vorticity. We choose the crystallographic axes of the altermagnet such that $K_{axx} = -K_{ayy} = K$ [21], and all other components of the tensor K are zero. The nonlinear magnetoelectric contribution stems from the circulating supercurrents around the vortex, and is given by:

$$\frac{M_a^{(\varphi)}}{M_0} = -m^2 \xi_{GL}^2 [(\partial_x \varphi)^2 - (\partial_y \varphi)^2] \\ = m^2 \xi_{GL}^2 \frac{x^2 - y^2}{r^4} \tanh^2 \left(\frac{r}{\xi_{GL}} \right), \quad (17)$$

where $M_0 = \frac{g\mu_B\nu_0 D |\Delta|^2}{8\pi^2 T^2 \xi_{GL}^2} K |\psi^{(2)}(\frac{1}{2} + \frac{\Gamma}{2\pi T})|$. The second contribution from the variation of $|\Delta|$ is:

$$\frac{M_a^{(|\Delta|)}}{M_0} = -\frac{\xi_{GL}^2}{|\Delta|^2} [(\partial_x |\Delta|)^2 - (\partial_y |\Delta|)^2] = -\frac{x^2 - y^2}{r^2 \cosh^4 \left(\frac{r}{\xi_{GL}} \right)}. \quad (18)$$

Interestingly, both contributions vanish along the nodal line of the altermagnet $|x| = |y|$, reflecting its d -wave symmetry. Moreover, the two contributions have opposite signs and, in amplitude, decay monotonically away from the vortex core, see Fig. 1(a)–(b). Nevertheless, the total magnetization $M = M_a^{(\varphi)} + M_a^{(|\Delta|)}$, in the case $m = 1$, exhibits a maximum at distances of the order of ξ_{GL} from the vortex core, see Fig. 1(c).

We can also evaluate the supercurrent to identify the contribution arising from the K_{ajk} term:

$$j_k = -\frac{\delta F}{\delta A} = 2 \left[c(\Delta \Pi_k^* \Delta^* + \Delta^* \Pi_k \Delta) + c' B_a K_{ajk} (\Delta \Pi_j^* \Delta^* + \Delta^* \Pi_j \Delta) \right]. \quad (19)$$

² Originally, in the published Ref. [10] a magnetoelectric effect linear in the phase gradient was suggested. The corresponding equations have later been corrected, see the latest arXiv version [33]. A similar linear magnetoelectric effect was reported in [34], which however appeared due to the use of an improper boundary condition. From simple symmetry arguments, see Eq. (10), a linear coupling between the phase gradient and the magnetization is not possible in superconducting altermagnets under equilibrium conditions.

This expression shows that, depending on the crystal orientation of the altermagnet, the term proportional to $B_a K_{ajk}$ can generate either a parallel or a perpendicular component of the supercurrent. For a phase gradient along the x direction and the orientation $K_{axx} = -K_{ayy} = K$, the induced contribution is parallel to the current. Notably, since this term is odd in B_a , the resulting current becomes asymmetric with respect to the magnetic field, such that $j_x(B_a) \neq j_x(-B_a)$. In contrast, for $K_{axy} = K_{ayx} = K$, a transverse component j_y arises, as discussed in Ref. [10].

Next to this, in the presence of an inhomogeneity of Δ , there is a free energy difference for opposite K_{ajk} :

$$F(K_{ajk}) - F(-K_{ajk}) = 2c' B_a K_{ajk} \Pi_j \Delta \Pi_k^* \Delta^*. \quad (20)$$

For example, in the presence of a phase gradient q , this expression reads $F(K_{ajk}) - F(-K_{ajk}) = 2c' B_a K_{ajk} q^2 |\Delta|^2$. The free energy difference is linear in K_{ajk} , *i.e.*, first order in the Néel vector, in a similar manner in which strain can introduce a term first order in the Néel vector [23–25, 36]. This shows that supercurrents, as well as magnitude gradients, can be used to aid the switching of the Néel vector of altermagnets using a magnetic field.

All these effects, so far considered for bulk superconducting altermagnets, can also appear in hybrid S/AM structures. In this case, inversion symmetry is broken, and there exists a polar vector normal to the interface, n_k . We can then construct a term, similar to the third term on the first line of Eq. (10), but now one of the spatial derivatives of the order parameter will be replaced by n_k , which may lead to a spatially dependent magnetic moment appearing in the AM. This is the focus of the next sections, where we analyze the proximity induced magnetization for S/AM and S/AM/S heterostructures beyond the GL limit, by solving the Usadel equation.

III. SUPERCONDUCTOR/ALTERMAGNET HETEROSTRUCTURES

In this section we consider hybrid S/AM and S/AM/S structures. We focus on a two-dimensional, single domain, d -wave collinear altermagnet. We denote the collinear axis as the z -direction in spin space ($a = 3$). In this case, the most general form of the K_{ajk} tensor is [21]:

$$K_{3jk} = \begin{pmatrix} K \cos(2\alpha) & K \sin(2\alpha) \\ K \sin(2\alpha) & -K \cos(2\alpha) \end{pmatrix}, \quad (21)$$

where α denotes the angle between the x axis and the crystallographic axis. Thus, we simplify the notation by introducing $K_{jk} \equiv K_{3jk}$. We consider that only one component of the spin-relaxation tensor $\Gamma \equiv \Gamma_{33}$ does not vanish, as this is the case in the low-energy model of Sec. IV.

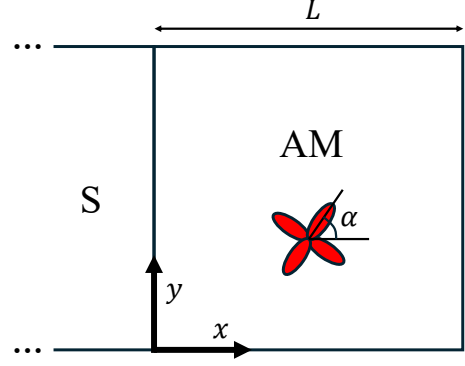


Figure 2. A square altermagnet of dimensions $L \times L$ next to an infinite (bulk) superconductor at $x = 0$. The remaining edges of the altermagnet ($x = L$, $y = 0$ and $y = L$) are bounded by vacuum. We draw a four-lobed red flower, reminiscent of d -wave symmetry, to represent the angle α between the x axis and the crystallographic axis of the altermagnet.

To investigate the proximity effect we need to solve Eq. (3). At the interface between the altermagnet and the superconductor, we impose the extended Kupriyanov–Lukichev boundary conditions [21, 37, 38]:

$$n_k \tilde{J}_k = \frac{D}{2\xi_0 \gamma_B} [\tilde{g}_S, \tilde{g}], \quad (22)$$

where \tilde{g}_S is the Green's function of the superconductor, \tilde{J} is defined in Eq. (4), n_k is the unit normal vector pointing outward from the altermagnet, $\Delta_0 = |\Delta(T=0)|$ is the zero temperature pair potential and $\xi_0 = \sqrt{D/\Delta_0}$ is the coherence length in the superconductor. For simplicity, we assume that the diffusive constant D is the same in both the superconductor and the altermagnet throughout this work. The constant γ_B characterizes the interface transparency:

$$\gamma_B = \frac{R_b \sigma_n}{\xi_0}, \quad (23)$$

with R_b the interface resistance per unit area and $\sigma_n = 2e^2 D \nu_0$ the Drude conductivity. At an interface with vacuum $\gamma_B \rightarrow \infty$.

We assume that the superconductor is not affected by the inverse proximity effect, and hence is described by the bulk BCS Green's function [28]:

$$\tilde{g}_S \approx \tilde{g}_{BCS} = \frac{1}{\sqrt{\omega^2 + |\Delta|^2}} (\omega \tilde{\tau}_3 + \tilde{\Delta}). \quad (24)$$

Furthermore, we assume a weak proximity effect, such that the Usadel equation in the AM can be linearized, as in Eq. (6). For a collinear axis along z , the pair amplitudes \hat{f} and $\hat{\tilde{f}}$ are diagonal in spin space:

$$\hat{f} = \begin{pmatrix} f_+ & 0 \\ 0 & f_- \end{pmatrix}, \quad \hat{\tilde{f}} = \begin{pmatrix} \tilde{f}_+ & 0 \\ 0 & \tilde{f}_- \end{pmatrix}. \quad (25)$$

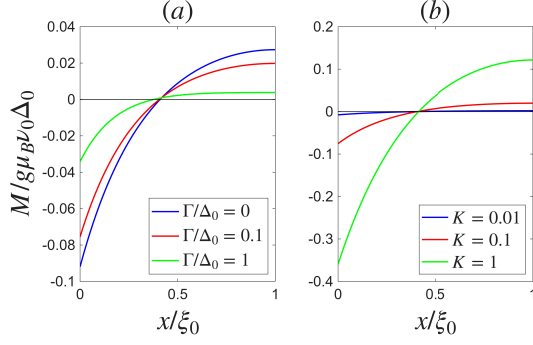


Figure 3. (a) Magnetization for $K = 0.1$ and different values of Γ . Increasing Γ suppresses the overall magnitude of the magnetization and reduces the characteristic decay length ξ . (b) Magnetization for $\Gamma/\Delta_0 = 0.1$ and varying K . A larger K enhances the induced magnetization. Around $x \approx \xi \approx 0.4\xi_0$, the magnetization changes sign, reflecting oscillations of the triplet component. The remaining parameters are $L = \xi_0$, $T/\Delta_0 = 0.1$, and $\gamma_B = 1$. The red line in both panels corresponds to the parameters of the low-energy model discussed in Sec. IV, with $h/\Delta_0 = 1$ and $\tau\Delta_0 = 0.1$.

Substituting this parametrization into the Usadel equation and neglecting nonlinear terms in the pair amplitudes yields:

$$(1 \pm i \operatorname{sgn}(\omega) K \cos(2\alpha)) \partial_x^2 f_{\pm} \pm 2i \operatorname{sgn}(\omega) K \sin(2\alpha) \partial_x \partial_y f_{\pm} + (1 \mp i \operatorname{sgn}(\omega) K \cos(2\alpha)) \partial_y^2 f_{\pm} = \frac{2(|\omega| + \Gamma)}{D} f_{\pm}, \quad (26)$$

and analogous equations are obtained for \tilde{f}_{\pm} by replacing $f_{\pm} \leftrightarrow \tilde{f}_{\pm}$.

In the following two subsections we solve Eq. (26), together with boundary conditions obtained by linearization of Eq. (22) for the S/AM bilayer and the S/AM/S Josephson junction (see Appendix B for details).

A. S/AM bilayer

We consider a square altermagnet of side L in contact with a bulk superconductor, as illustrated in Fig. 2.

For an arbitrary angle α , Eq. (26) must be solved numerically. However, for $\alpha = 0$ the problem becomes independent of the coordinate y , allowing for an analytic solution of the pair amplitudes:

$$f_{\pm} = \frac{|\Delta| \cosh(\kappa_{\omega}^{\pm}(x - L))}{\gamma_B \xi_0 \sqrt{\omega^2 + |\Delta|^2} (1 \pm i \operatorname{sgn}(\omega) K) \kappa_{\omega}^{\pm} \sinh(\kappa_{\omega}^{\pm} L)}, \quad (27)$$

with

$$\kappa_{\omega}^{\pm} = \sqrt{\frac{2(|\omega| + \Gamma)}{D(1 \pm i \operatorname{sgn}(\omega) K)}}. \quad (28)$$

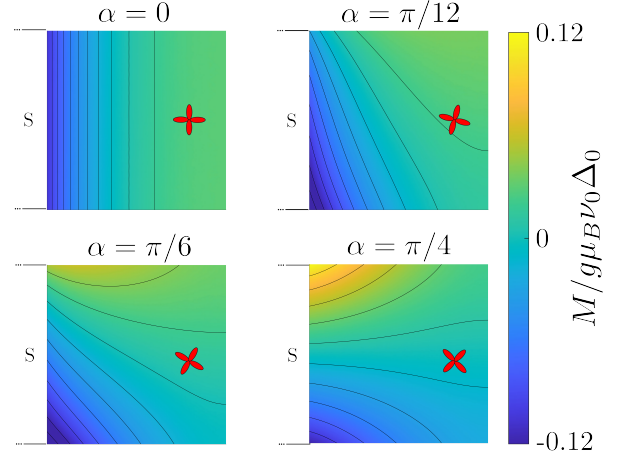


Figure 4. Magnetization in a 2D square altermagnet of side $L = \xi_0$ in contact with a superconductor for different values of α . For $\alpha = 0$, the induced magnetization is uniform along the y -direction and decays exponentially away from the interface. As α increases, a spatial redistribution of the magnetization emerges: negative magnetization localizes near the bottom-left corner, while positive magnetization develops near the top-left corner. At $\alpha = \pi/4$, d -wave symmetry dictates that the magnetization has equal magnitude and opposite sign in these two corners. For the other parameters we have chosen: $T/\Delta_0 = 0.1$, $\gamma_B = 1$, $K = 0.1$ and $\Gamma/\Delta_0 = 0.1$, which corresponds to $h/\Delta_0 = 1$ and $\tau\Delta_0 = 0.1$ in the low-energy model of Sec. IV.

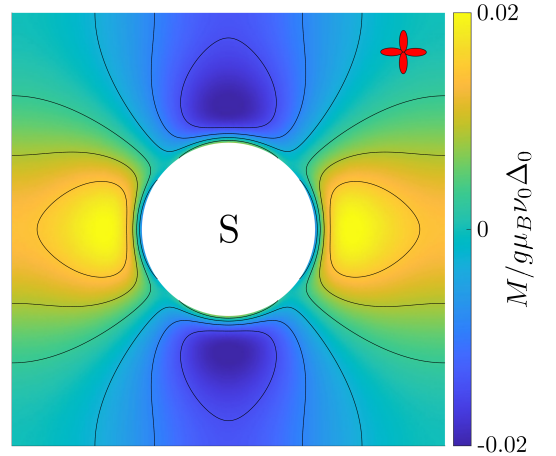


Figure 5. Circular superconducting island (white circle) of radius $r = \xi_0$ on top of a square altermagnet of side $L = 5\xi_0$. The underlying d -wave symmetry of the altermagnet becomes particularly evident, giving rise to four distinct lobes in the magnetization with alternating sign. Magnetization oscillations are especially prominent in this geometry. For instance, along the horizontal direction, the magnetization at the interface with the superconductor is initially negative (blue) and then oscillates to a bigger positive (yellow) lobe. For the other parameters we have chosen: $T/\Delta_0 = 0.1$, $\gamma_B = 1$, $K = 0.1$ and $\Gamma/\Delta_0 = 0.1$, which corresponds to $h/\Delta_0 = 1$ and $\tau\Delta_0 = 0.1$ in the low-energy model discussed in Sec. IV.

From these solutions, the characteristic decay length of the condensate is given by $\xi = \text{Re}(1/\kappa_\omega^\pm)$. If $K \ll 1$, the decay length reduces to $\xi \approx \sqrt{D/(2(|\omega| + \Gamma))}$ coinciding with the behavior expected for a conventional antiferromagnet [21, 39].

The parameter K introduces an imaginary component to the pair amplitudes in Eq. (27), thereby generating a finite triplet component of the condensate that decays over the length scale ξ . Its generation can be traced back to Eq. (16), where a spatial gradient of the order parameter induces a magnetization via the tensor K_{jk} . Consequently, these triplet correlations produce a

magnetization along the z axis, given by [21]:

$$M = \frac{1}{2} \nu_0 g \mu_B i \pi T \sum_{n=-\infty}^{\infty} \text{Tr}(\tilde{\tau}_3 \hat{\sigma}_3 \tilde{g}_{w_n}) \\ \simeq \nu_0 g \mu_B i \pi T \sum_{n=0}^{\infty} (f_- \tilde{f}_- - \tilde{f}_+ f_+) + O(f_+^2 \tilde{f}_+^2 - \tilde{f}_-^2 f_-^2). \quad (29)$$

Substituting the pair amplitudes from Eq. (27) yields:

$$M_{\alpha=0} = \frac{g \mu_B \nu_0 \pi T D |\Delta|^2}{\gamma_B^2 \xi_0^2} \sum_{n=0}^{\infty} \text{Im} \left(\frac{\cosh^2(\kappa_{\omega_n}^+ (x - L))}{(\omega_n + \Gamma)(\omega_n^2 + |\Delta|^2)(1 + iK) \sinh^2(\kappa_{\omega_n}^+ L)} \right), \quad (30)$$

where $\text{Im}(\cdot)$ denotes the imaginary part. Thus, a finite magnetization emerges in the altermagnet, decaying exponentially over a distance ξ . To illustrate this behavior, in Fig. 3 we plot the magnetization, determined by Eq. (30), for different values of K and Γ . As expected, the magnetization decreases monotonically with increasing Γ or decreasing K . Moreover, the magnetization exhibits a sign change at approximately $x \approx \xi$, a feature that is remarkably robust and persists even for very small K . Beyond this first sign change, additional oscillations may occur, although they are typically strongly suppressed due to the exponential decay.

In Fig. 4, we present numerical results for the magnetization for four different altermagnet orientations. For $\alpha = 0$ Eq. (30) applies and the magnetization

is uniform along y . As α increases, opposite-sign magnetization accumulates at the S/AM interface corners. At $\alpha = \pi/4$, the two corners carry equal but opposite sign magnetization, highlighting the underlying d -wave symmetry of the altermagnet.

The d -wave nature of the induced magnetization becomes even clearer if one considers a superconducting island of radius r deposited on an altermagnetic substrate, see Fig. 5. In this case, four lobes with alternating sign appear around the island, a remarkable manifestation of microscopic d -wave symmetry on the mesoscopic scale $\sim \xi$. In addition, the first sign change is more pronounced in this geometry.

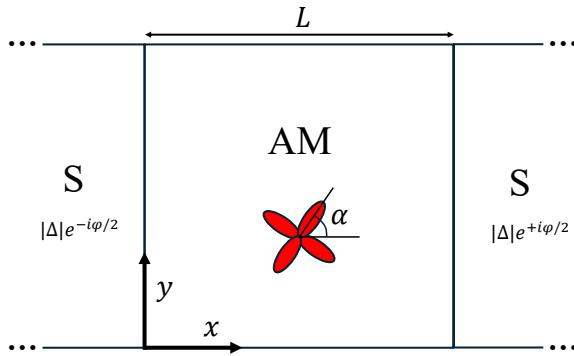


Figure 6. A square altermagnet of dimensions $[0, L] \times [0, L]$ sandwiched between two infinite (bulk) superconductors. At $x = 0$ the superconducting order parameter is $\hat{\Delta} = |\Delta|e^{-i\tilde{\tau}_3\varphi/2}$, while at $x = L$ it is $\hat{\Delta} = |\Delta|e^{i\tilde{\tau}_3\varphi/2}$, such that the total phase difference across the junction is φ . The remaining boundaries at $y = 0$ and $y = L$ are taken to be vacuum.

B. S/AM/S Josephson junction

We now consider a two-dimensional S/AM/S Josephson junction consisting of a square altermagnet of side length L sandwiched between two bulk (infinite) superconductors with a total phase difference φ , as illustrated in Fig. 6.

As in the case of the S/AM bilayer, solving Eq. (26) together with the boundary conditions for this case (see Appendix B2) generally requires numerical methods. However, for the orientation $\alpha = 0$, the problem becomes independent of the coordinate y , allowing for analytic solutions. In this case, the induced magnetization reads:

$$M_{\alpha=0} = \frac{g\mu_B\nu_0\pi TD|\Delta|^2}{\gamma_B^2\xi_0^2} \sum_{n=0}^{\infty} \text{Im} \left\{ \frac{[\cosh(\kappa_{\omega_n}^+ x) + \cosh(\kappa_{\omega_n}^+ (x-L))]^2 - 2(1 - \cos(\varphi)) \cosh(\kappa_{\omega_n}^+ x) \cosh(\kappa_{\omega_n}^+ (x-L))}{(\omega_n + \Gamma)(\omega_n^2 + |\Delta|^2)(1 + iK) \sinh^2(\kappa_{\omega_n}^+ L)} \right\}. \quad (31)$$

The expression inside the summation contains two distinct contributions. The first term in the curly brackets corresponds to the proximity induced magnetization (PIM) discussed for the S/AM bilayer, with contributions from both superconducting interfaces located at $x = 0$ and $x = L$. The second term, proportional to $1 - \cos(\varphi)$, represents the nonlinear magnetoelectric effect [10], in which a phase difference induces a magnetization. Importantly, the resulting magnetization is even in the superconducting phase difference, in contradiction to the claims made in Ref. [34]. An equilibrium phase-odd magnetization is

forbidden by symmetry [21, 40]. Consequently, from a symmetry perspective, this effect is distinct from the spin-splitting mechanisms that occur in the normal state.

In Fig. 7, we show numerical results for the magnetization at different crystallographic orientations. Near each interface the profile resembles the S/AM bilayer case from Fig. 4. For $\alpha = 0$ the magnetization is uniform along y , while for $\alpha = \pi/4$ a four-lobe structure with alternating sign emerges, reflecting the d -wave symmetry.

For $\alpha = 0$, one can also derive an analytic expression for the Josephson current:

$$j_x = \frac{\sigma_n}{2eD} i\pi T \sum_{n=0}^{\infty} \text{Tr}(\tilde{\tau}_3 \tilde{J}_x) = \frac{\sigma_n \pi T D |\Delta|^2}{e \gamma_B^2 \xi_0^2} \sin(\varphi) \sum_{n=0}^{\infty} \text{Re} \left(\frac{\kappa_{\omega_n}^+}{(\omega_n + \Gamma)(\omega_n^2 + |\Delta|^2) \sinh(\kappa_{\omega_n}^+ L)} \right). \quad (32)$$

A notable feature of Eq. (32) is the term $\sinh(\kappa_{\omega_n}^+ L)$ in the denominator, which can change sign because $\kappa_{\omega_n}^+$ is a complex number for $K \neq 0$. This sign reversal is indicative of $0-\pi$ transitions [41, 42]. Figure 8 illustrates this: the critical current I_c as a function of temperature T vanishes at a single point, consistent with a $0-\pi$ transition. The transition is most clearly visible for $\alpha = 0$ and becomes progressively suppressed as α increases. For $\alpha = \pi/8$ no transition occurs for the parameters we have chosen.

This angular dependence has a clear physical origin: the orientation $\alpha = 0$ maximizes the altermagnetic band splitting along the transport direction (x -axis),

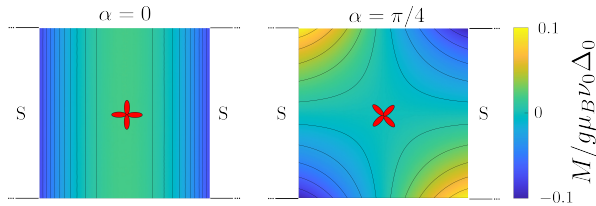


Figure 7. Magnetization in a square S/AM/S junction of side $L = \xi_0$. The phase difference between the two superconductors is $\varphi = \pi/2$. The magnetization near each interface resembles the bilayer case: it peaks at the interface and then decays exponentially. For $\alpha = 0$ the magnetization is y -independent and for $\alpha = \pi/4$ the magnetization at all four corners reaches equal magnitude with alternating sign, consistent with the underlying d -wave symmetry. For the other parameters we have chosen: $T/\Delta_0 = 0.1$, $\gamma_B = 1$, $K = 0.1$ and $\Gamma/\Delta_0 = 0.1$, which corresponds to $h/\Delta_0 = 1$ and $\tau\Delta_0 = 0.1$ in the low-energy model of Sec. IV.

thereby enhancing the mechanism responsible for the $0-\pi$ transition. In contrast, at $\alpha = \pi/4$, the altermagnetic bands are not spin-split along x , making a $0-\pi$ transition impossible even if one considers very large K .

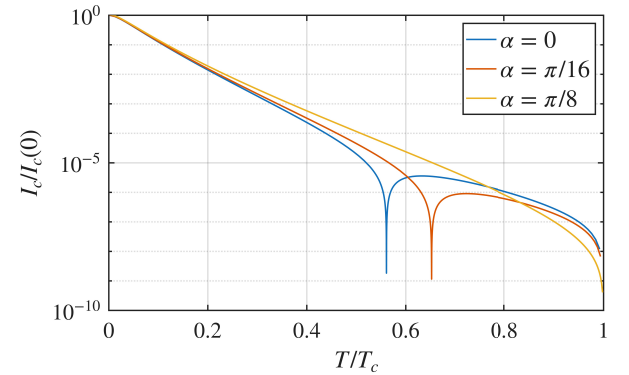


Figure 8. Critical current I_c in a S/AM/S rectangular junction of size $L_x = 10\xi_0$ and $L_y = \xi_0$ as a function of the temperature for different altermagnet orientations. A logarithmic scale was chosen for the vertical axis for clarity of presentation. For $\alpha = 0$ there is a sharp dip corresponding to a $0-\pi$ transition at $T/T_c \approx 0.56$ and for $\alpha = \pi/16$ at $T/T_c \approx 0.65$. Notably, for $\alpha = \pi/8$, superconductivity is suppressed before the transition can occur. For the other parameters we have chosen: $\gamma_B = 1$, $K = 0.2$ and $\Gamma/\Delta_0 = 0.2$ (which corresponds to $\tau\Delta_0 = 0.2$ and $h/\Delta_0 = 1$ in the low-energy model). The dependence of the order parameter on temperature is approximately given by [43]: $|\Delta| \approx \Delta_0 \tanh \left(1.74 \sqrt{T_c/T - 1} \right)$ with $T_c \approx 0.57\Delta_0$.

Previous studies have predicted $0 - \pi$ transitions in altermagnets for clean systems [8, 19]. However, to the best of our knowledge, here we show for the first time that this effect can persist even in the diffusive limit.

IV. LOW ENERGY EFFECTIVE MODEL

So far, all the results presented are obtained from the Usadel equation Eq. (3), which is valid for any altermagnet with disorder, independently of its microscopic details. What will change from one microscopic realization to another are the phenomenological constants K_{ajk} and Γ_{ab} .

In this section, to make a connection with previous works, we discuss the relation between the parameters of our model and those of a specific low-energy effective Hamiltonian when disorder is taken into account. Specifically, in Appendix A we derive the Usadel equation from a Bogoliubov–de Gennes (BdG) Hamiltonian describing a collinear d -wave altermagnet aligned along the z axis. This BdG Hamiltonian has been used in many works [8–12] to describe ballistic altermagnets:

$$\check{H}_{\text{BdG}}(\mathbf{r}) = \left[-\frac{\nabla_{\mathbf{r}}^2}{2m} - \mu \right] \check{\tau}_3 + \frac{h_{ij}}{2p_F^2} \hat{\sigma}_3 \partial_{r_i} \partial_{r_j} - \check{\Delta} + \check{V}_{\text{imp}}, \quad (33)$$

where h_{ij} is the anisotropic exchange field characterizing altermagnetism, and we have explicitly added the scattering potential \check{V}_{imp} due to nonmagnetic impurities.

In Appendix A, we show that an Usadel equation of the form given in Eq. (3) can be derived from the above Hamiltonian in the diffusive limit. For this particular realization, the tensor coefficients are related to the parameters of the Hamiltonian as follows:

$$K_{3jk} = \frac{6\tau}{d+2} h_{jk}, \quad \Gamma_{33} = \frac{2h^2\tau}{d(d+2)}, \quad T_{3jk} = \frac{h_{jk}}{2\mu}, \quad (34)$$

where τ is the elastic scattering time due to V_{imp} within the Born approximation, $h^2 = h_{ij}h_{ji}/2$, and d is the dimension of the sample. All components of the tensors that correspond to a spin index other than 3 vanish, consistent with previous symmetry arguments [21].

Notice that within this model, the tensors K_{ajk} and Γ_{ab} scale linearly with τ , analogous to the dependence of the anomalous Hall or spin–Hall conductivities on disorder in system with spin–orbit–coupling. Moreover, the tensor T_{3jk} , in contrast to K_{ajk} and Γ_{ab} , is of next leading order in the quasiclassical limit, as it is proportional to h/μ .

The spin–relaxation term $\Gamma_{33} \propto \tau$ describes a D’yakonov–Perel’-type mechanism [44]. Substituting this form into the self-consistency relation Eq. (15) shows that increasing disorder (*i.e.*, decreasing τ) enhances the critical temperature T_c , consistent with the predictions of Ref. [45]. It is worth emphasizing that the Γ tensor in our effective action, Eq. (2), is not bound to be related only

to this mechanisms, but it may have other contributions, as for example those studied in Refs. [39, 46].

Most of the results presented in Figs. (3–5, 7–8) are obtained for, $h/\Delta_0 = 1$, $\tau\Delta_0 = 0.1$, and low transparency interfaces, *i.e.* within the diffusive regime in this example. This demonstrates that the signatures of altermagnetism, such as the proximity induced magnetization, are also present in disordered systems. Naturally, in cleaner samples or with higher interface transparency, we expect these effects to become even more pronounced.

It should be noted that all the results above also apply qualitatively if, instead of an AM, one considers the proximity effect in a normal metal grown on top of an insulating AM. In the case of thin normal films, parameters such as the exchange field or the relaxation length take effective values that scale inversely with the film thickness, in analogy with superconductor–ferromagnetic insulator systems [20, 47].

V. CONCLUSIONS

In this article we investigate the interplay between superconductivity and altermagnetism, particularly in S/AM heterostructures. Starting from the Luttinger–Ward-type free energy functional, based on the nonlinear sigma model, we derive the corresponding Ginzburg–Landau free energy and identified two key contributions: a usual pair-breaking term stemming from a spin relaxation, and a higher order gradient term. The latter produces two distinct nonlinear effects. On the one hand, a magnetoelectric effect that generates a finite magnetization from a phase gradient. This effect is quadratic in the phase gradient and has been studied in ballistic systems in Refs. [9, 10]. On the other hand, a magnetic moment can also be generated by inhomogeneities of the modulus of the order parameter. This latter effect explains the proximity-induced magnetization predicted in Sec. III.

We also demonstrate that in S/AM heterostructures, superconducting correlations penetrating the altermagnet induce an equilibrium magnetization localized near the interface. This magnetization changes its sign over a length comparable to the coherence length. In S/AM/S Josephson junctions, both amplitude and phase gradients of Δ contribute to the magnetization, leading to the coexistence of the two effects. The Josephson current may also exhibit $0-\pi$ transitions, even in the diffusive regime.

In summary, our theory provides a foundation for studying the equilibrium and transport properties of disordered systems that combine superconductivity and altermagnetic order.

ACKNOWLEDGMENTS

R. H. and F. S. B. thank financial support from the the Spanish MCIN/AEI/10.13039/501100011033 through the grants PID2023-148225NB-C31, and TED2021-130292B-C41. F. S. B. also thanks financial support from the European Union's Horizon Europe research and innovation program under grant agreement No. 101130224 (JOSEPHINE).

I. V. T. acknowledges support from the Spanish MCIN/AEI/10.13039/501100011033 through the Project No. PID2023-148225NB-C32, and the Basque Government (Grant No. IT1453-22). T. K. acknowledges support by the Research Council of Finland through DYNCOR, Project Number 354735 and through the Finnish Quantum Flagship, Project Number 359240. S. I. is supported by the Research Council of Finland (Grant No. 355056).

-
- [1] L. Šmejkal, J. Sinova, and T. Jungwirth, *Phys. Rev. X* **12**, 040501 (2022).
 - [2] L. Šmejkal, J. Sinova, and T. Jungwirth, *Phys. Rev. X* **12**, 031042 (2022).
 - [3] R. Zarzuela, R. Jaeschke-Ubiergo, O. Gomonay, L. Šmejkal, and J. Sinova, *Phys. Rev. B* **111**, 064422 (2025).
 - [4] L. Šmejkal, A. B. Hellenes, R. González-Hernández, J. Sinova, and T. Jungwirth, *Phys. Rev. X* **12**, 011028 (2022).
 - [5] H. Reichlova, R. Lopes Seeger, R. González-Hernández, I. Kounta, R. Schlitz, D. Kriegner, P. Ritzinger, M. Lammel, M. Leiviskä, A. Birk Hellenes, *et al.*, *Nature Communications* **15**, 4961 (2024).
 - [6] M. Dou, X. Wang, and L. L. Tao, *Phys. Rev. B* **111**, 224423 (2025).
 - [7] Y.-F. Sun, Y. Mao, Y.-C. Zhuang, and Q.-F. Sun, *Phys. Rev. B* **112**, 094411 (2025).
 - [8] B. Lu, K. Maeda, H. Ito, K. Yada, and Y. Tanaka, *Phys. Rev. Lett.* **133**, 226002 (2024).
 - [9] J.-X. Hu, O. Matsyshyn, and J. C. W. Song, *Phys. Rev. Lett.* **134**, 026001 (2025).
 - [10] A. A. Zyuzin, *Phys. Rev. B* **109**, L220505 (2024).
 - [11] S. Chourasia, A. Svetogorov, A. Kamra, and W. Belzig, *Phys. Rev. B* **111**, 224503 (2025).
 - [12] L. Sharma and M. Thakurathi, *Phys. Rev. B* **112**, 104506 (2025).
 - [13] Y. Fukaya, K. Maeda, K. Yada, J. Cayao, Y. Tanaka, and B. Lu, *Phys. Rev. B* **111**, 064502 (2025).
 - [14] Y. Fukaya, B. Lu, K. Yada, Y. Tanaka, and J. Cayao, *Journal of Physics: Condensed Matter* **37**, 313003 (2025).
 - [15] S. Banerjee and M. S. Scheurer, *Phys. Rev. B* **110**, 024503 (2024).
 - [16] M. Papaj, *Phys. Rev. B* **108**, L060508 (2023).
 - [17] D. Chakraborty and A. M. Black-Schaffer, *Phys. Rev. B* **110**, L060508 (2024).
 - [18] C. Sun, A. Brataas, and J. Linder, *Phys. Rev. B* **108**, 054511 (2023).
 - [19] J. A. Ouassou, A. Brataas, and J. Linder, *Phys. Rev. Lett.* **131**, 076003 (2023).
 - [20] V. A. Bobkov, G. A. Bobkov, and I. V. Bobkova, *Inverse proximity effect in thin-film superconductor/magnet heterostructures with metallic and insulating magnets* (2025), [arXiv:2510.18102 \[cond-mat.supr-con\]](#).
 - [21] T. Kokkeler, I. Tokatly, and F. S. Bergeret, *SciPost Phys.* **18**, 178 (2025).
 - [22] T. Kokkeler, F. S. Bergeret, and I. V. Tokatly, *Phys. Rev. Lett.* **134**, 096001 (2025).
 - [23] I. E. Dzialoshinskii, *Sov. Phys. JETP* **6**, 621 (1958).
 - [24] H. Schiff, P. McClarty, J. G. Rau, and J. Romhányi, *Phys. Rev. Res.* **7**, 033301 (2025).
 - [25] M. Khodas, S. Mu, I. Mazin, and K. Belashchenko, *arXiv preprint arXiv:2506.06257* 10.48550/arXiv.2506.06257 (2025).
 - [26] A. I. Buzdin and M. Y. Kupriyanov, *JETP lett* **53**, 321 (1991).
 - [27] P. Virtanen, A. Vargunin, and M. Silaev, *Phys. Rev. B* **101**, 094507 (2020).
 - [28] F. S. Bergeret, A. F. Volkov, and K. B. Efetov, *Rev. Mod. Phys.* **77**, 1321 (2005).
 - [29] A. A. Abrikosov, *Fundamentals of the Theory of Metals* (Courier Dover Publications, 2017).
 - [30] R. M. White, *Quantum theory of magnetism: magnetic properties of materials* (Springer, 2007).
 - [31] M. Abramowitz and I. A. Stegun, *Handbook of mathematical functions: with formulas, graphs, and mathematical tables*, Vol. 55 (National Bureau of Standards Washington, DC, 2006).
 - [32] V. M. Edelstein, *Phys. Rev. Lett.* **75**, 2004 (1995).
 - [33] A. A. Zyuzin, *Magnetoelectric effect in superconductors with d-wave magnetization* (2025), [arXiv:2402.15459 \[cond-mat.supr-con\]](#).
 - [34] H. G. Gilil, B. Brekke, J. Linder, and A. Brataas, *Phys. Rev. B* **110**, L140506 (2024).
 - [35] A. Larkin and Y. N. Ovchinnikov, *Soviet Physics-JETP* **20**, 762 (1965).
 - [36] T. Aoyama and K. Ohgushi, *Phys. Rev. Mater.* **8**, L041402 (2024).
 - [37] M. Y. Kupriyanov and V. Lukichev, *Zh. Eksp. Teor. Fiz* **94**, 139 (1988).
 - [38] W. Belzig, F. K. Wilhelm, C. Bruder, G. Schön, and A. D. Zaikin, *Superlattices and Microstructures* **25**, 1251 (1999).
 - [39] E. H. Fyhn, A. Brataas, A. Qaiumzadeh, and J. Linder, *Phys. Rev. B* **107**, 174503 (2023).
 - [40] T. Kokkeler, T. T. Heikkilä, and F. S. Bergeret, *arXiv preprint arXiv:2510.11355* 10.48550/arXiv.2510.11355 (2025).
 - [41] L. Bulaevskii, V. Kuzii, and A. Sobyenin, *JETP lett* **25**, 290 (1977).
 - [42] V. V. Ryazanov, V. A. Oboznov, A. Y. Rusanov, A. V. Veretennikov, A. A. Golubov, and J. Aarts, *Phys. Rev. Lett.* **86**, 2427 (2001).
 - [43] M. Tinkham, *Introduction to superconductivity* (Courier Corporation, 2004).
 - [44] M. D'yakonov and V. Perel, *Soviet Journal of Experimental and Theoretical Physics* **33**, 1053 (1971).

- [45] M. M. Vasiakin and A. S. Mel'nikov, *Phys. Rev. B* **111**, L100502 (2025).
 [46] D. Sedov and M. S. Scheurer, *Quantum geometry and impurity sensitivity of superconductors without time-reversal symmetry: application to rhombohedral graphene and altermagnets* (2025), arXiv:2510.19943 [cond-mat.supr-con].
 [47] T. T. Heikkilä, M. Silaev, P. Virtanen, and F. S. Bergeret, *Progress in Surface Science* **94**, 100540 (2019).
 [48] P. Virtanen, F. Bergeret, and I. Tokatly, *Physical Review B* **105**, 224517 (2022).
 [49] W. Inc., Mathematica, Version 14.3 (2025).

Appendix A: Microscopic derivation of the Usadel equation

In this Appendix, we derive the Usadel equation for a superconductor with altermagnetic order. We will arrive at the result directly from the Gor'kov-Dyson equation, in contrast to the usual approach [38] where one first derives the Eilenberger equation and then obtains the Usadel equation by taking the diffusive limit. Our approach, although somewhat more complicated than the standard route, allows us to derive systematically and in a controlled way also the terms beyond the leading order in the quasiclassical approximation.

1. Gor'kov-Dyson equation

We consider a superconductor/altermagnet structure described by the following BdG Hamiltonian in the real space

$$\check{H}_{\text{BdG}}(\mathbf{r}) = \left[-\frac{\partial_{\mathbf{r}}^2}{2m} - \mu \right] \check{\tau}_3 + \frac{h_{ij}}{2p_F^2} \hat{\sigma}_3 \partial_{r_i} \partial_{r_j} - \check{\Delta} + \check{V}_{\text{imp}}. \quad (\text{A1})$$

For simplicity, we focus on the case $h_{xy} = h_{yx} = h \neq 0$, with $h_{ij} = 0$ otherwise. The Green's function \check{G} describing our system in the presence of disorder is determined from the Gor'kov-Dyson equation (GDE):

$$(i\omega_n - \check{H}_{\text{BdG}}(\mathbf{r}) - \check{\Sigma}_{\text{imp}}(\mathbf{r}))\check{G}(\mathbf{r}, \mathbf{r}') = \delta(\mathbf{r} - \mathbf{r}'), \quad (\text{A2})$$

where $\check{\Sigma}_{\text{imp}}$ is the impurity self-energy. To proceed, we go to the Wigner representation, $\check{G}(\mathbf{r}, \mathbf{r}') = \sum_{\mathbf{p}} e^{-i\mathbf{p}(\mathbf{r}-\mathbf{r}')} \check{G}_{\mathbf{p}}\left(\frac{\mathbf{r}+\mathbf{r}'}{2}\right)$, in which the GDE becomes:

$$\left(-\xi(\mathbf{p}) + \check{\Omega}(\mathbf{R}) + \check{H} \frac{p_x p_y}{p_F^2} + \frac{i}{2\tau} \check{\tau}_3 \bar{G}(\mathbf{R}) \right) e^{\frac{i}{2}(\check{\partial}_{\mathbf{R}} \vec{\partial}_{\mathbf{p}} - \check{\partial}_{\mathbf{p}} \vec{\partial}_{\mathbf{R}})} \check{\tau}_3 \check{G}_{\mathbf{p}}(\mathbf{R}) = 1. \quad (\text{A3})$$

Here, we introduced the center of mass coordinate $\mathbf{R} = \frac{\mathbf{r}+\mathbf{r}'}{2}$, $\check{\Omega}(\mathbf{R}) = (i\omega_n + \check{\Delta}(\mathbf{R}))\check{\tau}_3$, $\check{H} = h\hat{\sigma}_3\check{\tau}_3$ and $\xi(\mathbf{p}) = \frac{p^2}{2m} - \mu$. The last term in the parentheses in Eq. (A3) comes from the impurity self-energy in the self-consistent Born approximation, where the "bar" operation denotes integration over momenta $\bar{G}(\mathbf{R}) = \frac{i}{\pi\nu_0} \sum_{\mathbf{p}} \check{G}_{\mathbf{p}}(\mathbf{R})$. The right (left) arrows on top of the partial derivative operators mean that they only act to the right (left). Next, using the fact that the action of gradient operators in the exponent can be treated as translations, namely $A(\mathbf{p}, \mathbf{R}) e^{\frac{i}{2}(\check{\partial}_{\mathbf{R}} \vec{\partial}_{\mathbf{p}} - \check{\partial}_{\mathbf{p}} \vec{\partial}_{\mathbf{R}})} B(\mathbf{p}, \mathbf{R}) = A(\mathbf{p} - \frac{i}{2}\partial_{\mathbf{R}}, \mathbf{R} + \frac{i}{2}\partial_{\mathbf{p}}) B(\mathbf{p}, \mathbf{R})$, Eq. (A3) becomes:

$$\left[-\xi(\mathbf{p} - \frac{i}{2}\partial_{\mathbf{R}}) + \frac{\check{H}}{p_F^2} (p_x - \frac{i}{2}\partial_{R_x})(p_y - \frac{i}{2}\partial_{R_y}) + \check{\Omega}(\mathbf{R} + \frac{i}{2}\partial_{\mathbf{p}}) + \frac{i}{2\tau} \check{\tau}_3 \bar{G}(\mathbf{R} + \frac{i}{2}\partial_{\mathbf{p}}) \right] \check{\tau}_3 \check{G}_{\mathbf{p}}(\mathbf{R}) = 1. \quad (\text{A4})$$

To simplify upcoming calculations, it is convenient to introduce dimensionless parameters $\eta = 2\tau\xi(\mathbf{p})$ and $\psi = 1/(2\tau\mu)$, and the dimensionless Green's function $\check{\mathcal{G}}_{\mathbf{p}}(\mathbf{R}) = \frac{1}{2\tau} \check{\tau}_3 \check{G}_{\mathbf{p}}(\mathbf{R})$. Then, we obtain the dimensionless GDE:

$$\left[-\eta + il\sqrt{1+\eta\psi}n_i\partial_{R_i} + \frac{\psi l^2}{4}\partial_{\mathbf{R}}^2 + 2\tau\check{H}(n_x\sqrt{1+\eta\psi} - \frac{i\psi l}{2}\partial_{R_x})(n_y\sqrt{1+\eta\psi} - \frac{i\psi l}{2}\partial_{R_y}) \right. \\ \left. + 2\tau\check{\Omega}(\mathbf{R} + \frac{i}{2}\partial_{\mathbf{p}}) + i\bar{\mathcal{G}}(\mathbf{R} + \frac{i}{2}\partial_{\mathbf{p}}) \right] \check{\mathcal{G}}_{\mathbf{p}}(\mathbf{R}) = 1, \quad (\text{A5})$$

with $l = v_F\tau$, $\mathbf{n} = \mathbf{p}/|\mathbf{p}|$, and $p_i = \sqrt{2m(\mu + \xi)}n_i = p_F\sqrt{1 + \eta\psi}n_i$. The momentum averaging operation can now be represented as:

$$\bar{\mathcal{G}} = \frac{i}{\pi\nu_0} \int_{-1/\psi}^{\infty} d\eta \nu(\eta) \langle \mathcal{G} \rangle, \quad (\text{A6})$$

where the density of states is $\nu(\eta) = \nu_0(1 + \eta\psi)^{d/2-1}$, d is the dimension of the system, and $\langle \dots \rangle$ stands for averaging over the angles n_i . The momentum derivative can be written as $\partial_{p_i} = n_i \partial_p + \frac{1}{p}(\partial_{n_i} - n_i n_j \partial_{n_j})$, or, in dimensionless variables, $\partial_{p_i} = l \left(2n_i \sqrt{1 + \eta\psi} \partial_\eta + \psi \frac{\partial_{n_i} - n_i n_j \partial_{n_j}}{\sqrt{1 + \eta\psi}} \right)$.

2. Gradient expansion and diffusive limit

We next assume the quasiclassical approximation and the diffusive limit, meaning that the following hierarchy of energy scales holds $\mu \gg \tau^{-1} \gg |\Delta|, h$. Within these assumptions, the dimensionless parameter ψ is small. In the quasiclassical theory one usually keeps only the leading order in ψ (ψ^0) [38], but here, for completeness, we will also retain terms of the next order (ψ^1).

The quasiclassical approximation allows us to do the gradient expansion. We will retain terms up to the second order in spatial gradients ∂_{R_i} , namely $\check{\mathcal{G}}(\mathbf{R} + \frac{i}{2}\partial_{\mathbf{p}}) \approx \check{\mathcal{G}} + \frac{i}{2}\check{\mathcal{G}}_i \partial_{p_i} - \frac{1}{8}\check{\mathcal{G}}_{ij} \partial_{p_i} \partial_{p_j}$, and similarly for $\check{\Omega}(\mathbf{R} + \frac{i}{2}\partial_{\mathbf{p}})$. Here we use the notation $\check{\mathcal{G}}_i = \partial_{R_i} \check{\mathcal{G}}$, $\check{\mathcal{G}}_{ij} = \partial_{R_i} \partial_{R_j} \check{\mathcal{G}}$. Then, after some rearranging, the GDE can be rewritten as:

$$(-\eta + i\bar{\mathcal{G}})\check{\mathcal{G}} = 1 - \left[2\check{\Omega}\tau\check{\mathcal{G}} + \frac{i}{2}(2\tau\check{\Omega}_i + i\bar{\mathcal{G}}_i)\partial_{p_i}\check{\mathcal{G}} - \frac{1}{8}(2\tau\check{\Omega}_{ij} + i\bar{\mathcal{G}}_{ij})\partial_{p_i}\partial_{p_j}\check{\mathcal{G}} + il\sqrt{1 + \eta\psi}n_i\check{\mathcal{G}}_i + \frac{\psi l^2}{4}\check{\mathcal{G}}_{ii} \right. \\ \left. + 2\tau\check{H}n_x n_y(1 + \eta\psi)\check{\mathcal{G}} - i\psi l\tau\check{H}\sqrt{1 + \eta\psi}(n_x\check{\mathcal{G}}_y + n_y\check{\mathcal{G}}_x) \right]. \quad (\text{A7})$$

Next, we expand the Green's function in parameters $l\partial_R$, $\tau\check{\Omega}$ and $\tau\check{H}$, all of which are small in the diffusive limit:

$$\check{\mathcal{G}} = \check{\mathcal{G}}^{(0)} + \check{\mathcal{G}}^{(1)} + \check{\mathcal{G}}^{(2)} + \check{\mathcal{G}}^{(3)} + \dots, \quad (\text{A8})$$

where n in $\check{\mathcal{G}}^{(n)}$ denotes the order in small parameters. From Eq. (A7), we see that the zeroth-order contribution is given as:

$$\check{\mathcal{G}}^{(0)} = (-\eta + i\bar{\mathcal{G}}^{(0)})^{-1}. \quad (\text{A9})$$

Similarly, we can write equations for higher-order components. For $k \geq 1$, we have:

$$\check{\mathcal{G}}^{(k)} + i\check{\mathcal{G}}^{(0)}\bar{\mathcal{G}}^{(k)}\check{\mathcal{G}}^{(0)} = X^{(k)}, \quad (\text{A10})$$

with:

$$X^{(k)} = -\check{\mathcal{G}}^{(0)} \left[-i\theta_{k-s-1}\bar{\mathcal{G}}^{(s)}\check{\mathcal{G}}^{(k-s)} + 2\tau\check{\Omega}\check{\mathcal{G}}^{(k-1)} + i\theta_{k-2}\tau\check{\Omega}_i\partial_{p_i}\check{\mathcal{G}}^{(k-2)} - \frac{\theta_{k-s-1}}{2}\bar{\mathcal{G}}^{(s)}\partial_{p_i}\check{\mathcal{G}}^{(k-s-1)} \right. \\ \left. - \frac{\theta_{k-3}}{4}\tau\check{\Omega}_{ij}\partial_{p_i}\partial_{p_j}\check{\mathcal{G}}^{(k-3)} - \frac{i\theta_{k-s-2}}{8}\bar{\mathcal{G}}^{(s)}\partial_{p_i}\partial_{p_j}\check{\mathcal{G}}^{(k-s-2)} + il\sqrt{1 + \eta\psi}n_i\check{\mathcal{G}}^{(k-1)} + \frac{\theta_{k-2}\psi l^2}{4}\check{\mathcal{G}}_{ii}^{(k-2)} \right. \\ \left. + 2\tau\check{H}n_x n_y(1 + \eta\psi)\check{\mathcal{G}}^{(k-1)} - i\theta_{k-2}\psi l\tau\check{H}\sqrt{1 + \eta\psi}(n_x\check{\mathcal{G}}_y^{(k-2)} + n_y\check{\mathcal{G}}_x^{(k-2)}) \right], \quad (\text{A11})$$

where we introduced the discrete step function $\theta_i = \begin{cases} 1, & i \geq 0, \\ 0, & i < 0. \end{cases}$, and $s \geq 0$ is an internal summation variable (summation over repeated indices is assumed).

3. Solution procedure

To solve Eq. (A7), we will exploit the fact that the momentum-averaged Green's function $\bar{\mathcal{G}}$ of a diffusive system can be always written in the form $\bar{\mathcal{G}} = Q + B$, so that $Q^2 = 1$ and $[B, Q] = 0$ [48]. Namely, Q is the part of the Green's function that is normalized to 1, and B is known as the longitudinal correction. We can expand B up to third order in the small diffusive parameters, in the same way as in Eq. (A8): $B \approx B^{(0)} + B^{(1)} + B^{(2)} + B^{(3)}$.

For clarity, in the following we will focus on 3D systems. Let us start by calculating $\check{\mathcal{G}}^{(0)}$. We first assume that $B^{(0)}$ vanishes, which will be justified *a posteriori*. Then, from Eq. (A9) we find $\check{\mathcal{G}}^{(0)} = (-\eta + iQ)^{-1} = -(\eta + iQ)/(\eta^2 + 1)$.

We can now calculate $\bar{\mathcal{G}}^{(0)}$ by placing this expression into Eq. (A6). The resulting integral, as well as all other energy integrals we will encounter in the upcoming calculations, can be solved using residues [48]:

$$\int_{-1/\psi}^{\infty} (1 + \eta\psi)^{d/2-1} \frac{(1 + \eta\psi)^m \eta^n}{(1 + \eta^2)^p} = 2\pi i \sum_{\pm} \text{Res}_{\eta=\pm i} q(\eta) \frac{(1 + \eta\psi)^m \eta^n}{(1 + \eta^2)^p}. \quad (\text{A12})$$

The above expression is valid for all convergent integrals (d, m, n, p are non-negative integers), and we introduced the function

$$q(\eta) = \begin{cases} \frac{i}{2\pi} \ln(-1 - \eta\psi)(1 + \eta\psi)^{d/2-1}, & d \text{ even} \\ \frac{i}{2} \sqrt{-1 - \eta\psi}(1 + \eta\psi)^{d/2-3/2}, & d \text{ odd.} \end{cases} \quad (\text{A13})$$

Note that the Q -independent part of $\check{\mathcal{G}}^{(0)}$ gives a divergence upon integration, but this divergence can be regularized by gauge-invariance arguments [48]. Finally, expanding the result of the integration in ψ , we get $\bar{\mathcal{G}}^{(0)} = Q + O(\psi^2)$. This justifies our earlier assumption that $B^{(0)} = 0$. From here, we also see that $B^{(i)} = \bar{\mathcal{G}}^{(i)}$ ($i = 1, 2, 3, \dots$).

We proceed to calculate the higher-order components, $\check{\mathcal{G}}^{(i)}$, $i = 1, 2, 3$. From Eqs. (A10) and (A11), we have $\check{\mathcal{G}}^{(i)} + i\check{\mathcal{G}}^{(0)}B^{(i)}\check{\mathcal{G}}^{(0)} = X^{(i)}$. We then apply the momentum averaging operation (A6) to this expression, and expand up to first order in ψ , to get $B^{(i)} + \frac{1}{2}(QB^{(i)}Q - B^{(i)}) - \frac{i\psi}{4}\{Q, B^{(i)}\} = \bar{X}^{(i)}$. Then, using $Q^2 = 1$ and $[B^{(i)}, Q] = 0$, this is simplified to:

$$B^{(i)} = \bar{X}^{(i)} + \frac{i\psi}{4}(Q\bar{X}^{(i)} + \bar{X}^{(i)}Q), \quad (\text{A14})$$

which is valid up to order ψ^1 . Finally, we can express $\check{\mathcal{G}}^{(i)}$ as:

$$\check{\mathcal{G}}^{(i)} = X^{(i)} - i\check{\mathcal{G}}^{(0)}B^{(i)}\check{\mathcal{G}}^{(0)}. \quad (\text{A15})$$

The Usadel equation is obtained from the condition that the longitudinal part commutes with Q , namely:

$$\frac{1}{2\tau} \sum_i [B^{(i)}, Q] = 0, \quad (\text{A16})$$

where the prefactor $1/2\tau$ is added to get the standard form of the Usadel equation.

4. Final solution and the Usadel equation

The procedure described above is straightforward, but it produces a large number of terms, which we handle using symbolic computation software, *Wolfram Mathematica* [49]. In the following, we write the final result of this calculation. In the first order in small expansion parameters we get:

$$\frac{1}{2\tau} [B^{(1)}, Q] = [Q, i\check{\Omega}]. \quad (\text{A17})$$

This is the standard commutator contribution to the Usadel equation. Similarly, in the second order in small parameters we have:

$$\frac{1}{2\tau} [B^{(2)}, Q] = -D\partial_{R_i}(Q\partial_{R_i}Q) - \frac{\Gamma}{2}[Q, \hat{\sigma}_3\check{\tau}_3Q\hat{\sigma}_3\check{\tau}_3], \quad (\text{A18})$$

where $D = \frac{1}{d}v_F^2\tau$ is the diffusion constant, and $\Gamma = \frac{2h^2\tau}{d(d+2)}$ is the relaxation rate. Here we can recognize the standard current term, and the D'yakonov-Perel-like spin-relaxation term. In the third order in the expansion we find

$$\begin{aligned} \frac{1}{2\tau} [B^{(3)}, Q] = & -\frac{3iD\tau}{2(d+2)} h_{ij} \partial_{R_i} [\hat{\sigma}_3\check{\tau}_3 + Q\hat{\sigma}_3\check{\tau}_3Q, \partial_{R_j}Q] + \frac{D\tau\psi}{4} h_{ij} \partial_{R_i} \{\hat{\sigma}_3\check{\tau}_3 + Q\hat{\sigma}_3\check{\tau}_3Q, Q\partial_{R_j}Q\} \\ & - \frac{3iD\tau}{2(d+2)} h_{ij} [\hat{\sigma}_3\check{\tau}_3, Q\partial_{R_i}Q\partial_{R_j}Q] - \frac{D\tau\psi}{4} h_{ij} [\hat{\sigma}_3\check{\tau}_3, \partial_{R_i}Q\partial_{R_j}Q]. \end{aligned} \quad (\text{A19})$$

In writing the above equations, we have kept only the leading-order contribution proportional to $\check{\Omega}$ that appears in $B^{(1)}$. The $\check{\Omega}$ -dependent terms that appear in $B^{(2)}$ and $B^{(3)}$ were omitted for simplicity, since they are not relevant for the phenomena discussed here.

Collecting the above results yields the final Usadel equation, $\frac{1}{2\tau}[B^{(1)} + B^{(2)} + B^{(3)}, Q] = 0$, which has a form specified in Eq. (3) with the coefficients given in Eq. (34). The generalization from the case discussed in this Appendix with only $h_{xy} = h_{yx} = h \neq 0$ to Eq. (34), valid for any orientation, follows from rotational invariance of the tensor h_{ij} .

We note that the coefficients appearing in the third-order gradient contribution scale as $h_{ij}D\tau$ and $h_{ij}D\tau\psi$, respectively. This disagrees with an earlier derivation of the Usadel equation for altermagnets in the weak-proximity limit, $Q \approx \tilde{\tau}_3 + \begin{bmatrix} 0 & \hat{f} \\ \hat{f} & 0 \end{bmatrix}$, reported in Ref. [34], where the corresponding coefficients were found to scale instead as $h_{ij}D\tau\psi^2 \ll h_{ij}D\tau$ and $h_{ij}D\tau\psi$. The origin of this discrepancy lies in the truncation of the spherical-harmonic expansion of \hat{f} in Ref. [34]. Only the first angular harmonic was retained, whereas the second harmonic is also required and couples directly to the d -wave (second spherical harmonic) altermagnetic field. As a consequence, Ref. [34] omitted a leading-order contribution to one of the coefficients.

Appendix B: Linearized Boundary Conditions

In Section III of the main text, we solve the linearized Usadel equation, Eq. (26) in a rectangular geometry where $(x, y) \in [0, L] \times [0, L]$. In this Appendix we present the boundary conditions that complement the linearized equations which originate by substituting the parametrization Eq. (6) into the Kupriyanov–Lukichev boundary condition Eq. (22) and retaining only terms linear in the pair amplitudes. Like in Sec. III in the main text, we parameterize the altermagnet tensor K_{ajk} by a single magnitude K and angle α as in Eq. (21). For the S/AM case (setup shown in Fig. 2 of the main text), to linear order in $1/\gamma_B$, we obtain:

$$(1 \pm i \operatorname{sgn}(\omega)K \cos(2\alpha))\partial_x f_{\pm} \pm i \operatorname{sgn}(\omega)K \sin(2\alpha)\partial_y f_{\pm} = -\frac{|\Delta|}{\gamma_B \xi_0 \sqrt{\omega^2 + |\Delta|^2}}, \quad x = 0 \quad (\text{B1a})$$

$$(1 \pm i \operatorname{sgn}(\omega)K \cos(2\alpha))\partial_x f_{\pm} \pm i \operatorname{sgn}(\omega)K \sin(2\alpha)\partial_y f_{\pm} = 0, \quad x = L \quad (\text{B1b})$$

$$(1 \mp i \operatorname{sgn}(\omega)K \cos(2\alpha))\partial_y f_{\pm} \pm i \operatorname{sgn}(\omega)K \sin(2\alpha)\partial_x f_{\pm} = 0, \quad y = 0, L \quad (\text{B1c})$$

with analogous boundary conditions for \tilde{f}_{\pm} .

For the S/AM/S Josephson junctions (see Fig. 6 of the main text), to linear order in $1/\gamma_B$, we obtain:

$$(1 \pm i \operatorname{sgn}(\omega)K \cos(2\alpha))\partial_x f_{\pm} \pm i \operatorname{sgn}(\omega)K \sin(2\alpha)\partial_y f_{\pm} = -\frac{|\Delta|e^{i\varphi/2}}{\gamma_B \xi_0 \sqrt{\omega^2 + |\Delta|^2}}, \quad x = 0 \quad (\text{B2a})$$

$$(1 \pm i \operatorname{sgn}(\omega)K \cos(2\alpha))\partial_x f_{\pm} \pm i \operatorname{sgn}(\omega)K \sin(2\alpha)\partial_y f_{\pm} = \frac{|\Delta|e^{-i\varphi/2}}{\gamma_B \xi_0 \sqrt{\omega^2 + |\Delta|^2}}, \quad x = L \quad (\text{B2b})$$

$$(1 \mp i \operatorname{sgn}(\omega)K \cos(2\alpha))\partial_y f_{\pm} \pm i \operatorname{sgn}(\omega)K \sin(2\alpha)\partial_x f_{\pm} = 0, \quad y = 0, L \quad (\text{B2c})$$

$$(1 \pm i \operatorname{sgn}(\omega)K \cos(2\alpha))\partial_x \tilde{f}_{\pm} \pm i \operatorname{sgn}(\omega)K \sin(2\alpha)\partial_y \tilde{f}_{\pm} = -\frac{|\Delta|e^{-i\varphi/2}}{\gamma_B \xi_0 \sqrt{\omega^2 + |\Delta|^2}}, \quad x = 0 \quad (\text{B2d})$$

$$(1 \pm i \operatorname{sgn}(\omega)K \cos(2\alpha))\partial_x \tilde{f}_{\pm} \pm i \operatorname{sgn}(\omega)K \sin(2\alpha)\partial_y \tilde{f}_{\pm} = \frac{|\Delta|e^{i\varphi/2}}{\gamma_B \xi_0 \sqrt{\omega^2 + |\Delta|^2}}, \quad x = L \quad (\text{B2e})$$

$$(1 \mp i \operatorname{sgn}(\omega)K \cos(2\alpha))\partial_y \tilde{f}_{\pm} \pm i \operatorname{sgn}(\omega)K \sin(2\alpha)\partial_x \tilde{f}_{\pm} = 0, \quad y = 0, L. \quad (\text{B2f})$$

We solved the linearized Usadel equation, Eq. (26), together with these boundary conditions to obtain the results in Figs. 3-8 in the main text.